Long-Term Persistence of Rayleigh Signature of Optical Fibers in Harsh Environment

Luca Schenato, *Member, IEEE*, Martina Cappelletti, Daniele Orsuti, Andrea Galtarossa, *Life Fellow, IEEE*, Marco Santagiustina, *Member, IEEE*, Simonetta Cola, and Luca Palmieri, *Senior Member, IEEE*

***Abstract*—This article investigates the persistence of Rayleigh signatures in optical sensing fibers installed in harsh environments. We show that the measurements taken from some fibers installed in rough conditions still retain the Rayleigh signature after more than six years, even though those measurements have been collected with different Optical Frequency Domain Reflectometry interrogators and setups. To this aim, we rely on the Spectral Correlation Analysis, which compares and spectrally correlates the fiber's Rayleigh-backscattered trace despite the usage of different interrogator and their spatial misalignment.**

***Index Terms*—Optical frequency domain reflectometry, Rayleigh scattering, Rayleigh signature.**

I. Introduction

THE phenomenon of Rayleigh scattering in single-mode optical fibers can be modeled as a random variable with a relatively small amplitude. It is caused by unpredictable fluctuations in the refractive index, which is frozen during the fiber drawing. Essentially, the scattering occurs due to isolated scattering centers that are randomly distributed throughout the fiber. These centers cause the forward and backward propagating modes to couple together and interfere, as described by the Coupled-Mode Theory [1], [2].

Despite being randomly distributed, scattering centers are permanently frozen during the fiber drawing process, creating a unique "signature" of each fiber, which can be exploited, for example, to identify that fiber univocally. The potential of this feature in secure network applications has been evident since the early 2000s [3]. It has been then rediscovered and proposed again over the years, either directly [4] or in conjunction with the definition of Rayleigh-based unclonable optical fiber identification [5].

At the same time, that signature undergoes local scaling when the fiber is perturbed, for example, by a change in strain and temperature. In such a way, the Rayleigh signature keeps track of strain and temperature variation and can be exploited in high spatial resolution distributed sensing. For example, this mechanism is at the basis of Optical Frequency Domain Reflectometry (OFDR). Accordingly, when an external perturbation is applied, it causes a traceable modification of the Rayleigh signature in the form of a deterministic shift of its spectrum. Given the faint intensity of the Rayleigh backscatter signal, cross-correlating the spectrum of a perturbed section of the optical fiber with the spectrum of the same section when not perturbed is the most effective way to measure the perturbation-induced shift [6].

This approach has led to the development of successful OFDR commercial platforms capable of highly dense distributed strain and temperature measurements under mostly static conditions [7], [8], which, over the years, have been used in various fields of application and have proven to be very effective. Practically, this involves relying on proprietary software to cross-correlate the spectra and using the same patchcord, or sequence of patchcords, to connect the same interrogator to the sensing fiber. Even within this framework, recovering spectral shifts from raw optical Rayleigh backscattering data is critical for OFDR measurements conducted in harsh environments and, as a matter of fact, has posed limits to the broad applicability of OFDR in such applications. This issue has pushed the community to propose alternative approaches based on filtering the correlation spectra based on the quality of the correlation itself, yet with mixed success [9], [10], [11]. To the authors' knowledge, all the test cases and examples cited in the literature were carried out over a short time period, with the same interrogator and identical optical setup, and, mostly, in relatively mild conditions.

Indeed, when different setups and interrogators are used, it is necessary to manually cross-correlate the Rayleigh signature spectra. This process depends on the persistence of the Rayleigh signature, regardless of the time elapsed since the reference was taken or the setup used. About this, in 2013, Froggatt and Gifford showed that the amplitude of the Rayleigh backscatter signal along the fiber remained almost unchanged for two years under favorable conditions, i.e., a single spool of fiber kept wound and undisturbed in the lab [12]. However, there has been no

Manuscript received 15 March 2024; revised 24 May 2024; accepted 11 June 2024. Date of publication 13 June 2024; date of current version 16 September 2024. This work was supported in part by the European Union under the Italian National Recovery and Resilience Plan (NRRP) of NextGenerationEU, partnership on Telecommunications of the Future (PE0000001 - program "RESTART") and MIUR (Project PRIN – 2022HFWMPC - Debris Phos). *(Corresponding author: Luca Schenato.)*

Luca Schenato, Martina Cappelletti, and Daniele Orsuti are with the Department of Information Engineering, University of Padova, I-35131 Padua, Italy (e-mail: luca.schenato@unipd.it).

Andrea Galtarossa, Marco Santagiustina, and Luca Palmieri are with the Department of Information Engineering, University of Padova, I-35131 Padua, Italy, and also with the National Inter-University Consortium for Telecommunications–CNIT, 43124 Parma, Italy (e-mail: luca.schenato@unipd.it).

Simonetta Cola is with the Department of Civil, Environmental and Architectural Engineering, University of Padova, I-35129 Padua, Italy.

Color versions of one or more figures in this article are available at https://doi.org/10.1109/JLT.2024.3414254.

Digital Object Identifier 10.1109/JLT.2024.3414254

report on the persistence of Rayleigh backscatter in long-term measurements on fibers collected with different interrogators and setups. We believe this feature is crucial in those applications requiring long-term measurements, such as those in harsh environments, during which the interrogator and setup may need to be replaced, substituted, or repaired.

This study, extending a preliminary work reported in [13], explores the feasibility of consistent OFDR monitoring over an extended period and in such challenging conditions. To achieve this, we have collected data from fibers installed in two different sites: at a bridge, where the fibers were integrated within a foundation pile, and at a landslide slope, where the fibers were embedded in soil anchors. In both sites, we compare the Rayleigh signature spectra of recent measurements to a reference Rayleigh spectrum measured up to five years before using a different interrogator and connecting patchcords. To ensure accuracy and reliability, we have implemented the spectral correlation analysis technique presented in [14] and initially proposed by Froggatt et al. [6], which allows us to successfully link the spectra and establish the consistency of the OFDR monitoring technique over an extended period, independently by the apparatus and setup used in the measurements.

Our results confirm that the OFDR monitoring technique remains reliable and accurate over an extended period of time, as testified by the high quality of the correlation of the most recent traces with the reference measurement after more than six years, even in unfavorable conditions. Furthermore, our study highlights the importance of proper spectral correlation analysis in ensuring the consistency of the measurements.

II. Spectral Correlation Analysis of OFDR Traces Collected With Different Setups

In general, an OFDR device measures the roundtrip frequency response of the fiber, which is determined by the Rayleigh scattering. The frequency response, $R(\omega)$, collected at the input of a fiber probed by an ideal optical pulse, is given by the coherent contributions of the light that is reflected at the randomly distributed discrete scattering centers of the fiber [2]. Ignoring polarization effects, it reads

$$R(\omega) = \sum_k \rho_k \exp\left(-\jmath \frac{2\omega n z_k}{c_0}\right), \tag{1}$$

where z_k and ρ_k are the positions and complex reflection coefficients of the k-th scattering center of the fiber, $\omega = 2\pi f$ is the optical angular freqeuncy, c_0 is the speed of light in the vacuum, and n is the effective refractive index of the propagating mode.

Please note that z_k, ρ_k of (1) are random variables. Nonetheless, a single realization of them is frozen at drawing, and as long as no significant perturbation acts on the fiber, it remains unchanged. That single realization of z_k, ρ_k is therefore associated with a specific frequency response $R(\omega)$, uniquely identifying that fiber and constituting its so-called Rayleigh signature or fingerprint.

At the same time, the phase term $2\omega n z_k/c_0$ of (1) highlights an important feature of the frequency response. Given that the phase term joins together ω and n, $R(\omega)$ is invariant, at the first order, for any changes Δn and $\Delta\omega$ of the effective refractive index and the angular frequency shift, which satisfy

$$\Delta\omega \approx \frac{\Delta n}{n}\omega. \tag{2}$$

According to (2), repeated measurements of $R(\omega)$ of the same physical section of the fiber, collected in different perturbation states (i.e., for varying Δn among the measurement), originate spectrally-shifted versions of the same signature. This common mechanism is exploited in Rayleigh-based distributed fiber sensing to calculate temperature- or strain-induced refractive index changes along the fiber [2], [6]. Practically, the temperature and strain variation, ΔT and $\Delta\varepsilon$, are linearly related to the equivalent spectral shift $\Delta f = \Delta\omega/2\pi$ through the gage factors k_T and k_ε, as [15], [16], [17]:

$$\Delta f = \frac{\Delta\omega}{2\pi} = k_T \Delta T + k_\varepsilon \Delta\varepsilon \tag{3}$$

where

$$k_T \approx -1.25\,\mathrm{GHz}/^\circ\mathrm{C}, \qquad k_\varepsilon \approx -150\,\mathrm{MHz}/\mu\varepsilon. \tag{4}$$

Finally, neglecting the chromatic dispersion, the roundtrip impulse response, i.e., the inverse Fourier transform of the frequency response of from (1), is given by:

$$r(t) = \sum_k \rho_k \exp\left(-\jmath \frac{2\,\omega_0\, n\, z_k}{c_0}\right) \delta\left(t - 2\frac{z_k}{v_g}\right), \tag{5}$$

where δ is the Dirac delta function, v_g is the group velocity, and $\omega_0 = 2\pi f_0$ is the central angular frequency around which the measurement over a given bandwidth is performed. Moreover, here, the sum is carried out over the scattering centers of the whole fiber. The signal $r(t)$ represents the raw optical trace collected by OFDR devices. By time-windowing $r(t)$ over an arbitrary interval $\mathcal{T} = [t_0, t_0 + T_g]$, with duration T_g, it is possible to isolate the contribution of the backscattered light originating within the fiber section $\mathcal{Z} = \mathcal{T} v_g$, and therefore determine its the local signature.

Following this approach, start by considering two subsequent measurements of the roundtrip impulse response $r_{\text{ref}}(t)$ and $r_{\text{meas}}(t)$ of the fiber under test, in unperturbed and perturbed states, respectively. In these expressions, the roundtrip time t can be converted into the distance z along the fiber as $z = tc_0/(2n)$. We will refer to those traces as the reference and measurement trace for simplicity.

In this work, we have implemented the so-called Spectral Correlation Analysis (SCA) to track the local spectral shift along the fiber [14].

This method, schematically represented in Fig. 1, consists of the following steps:

- For a given time window of duration T_g, and for each time t and arbitrary time delay $\Delta\tau$, consider the time window $\mathcal{T}_{\text{ref}} = [t, t + T_g]$ and its $\Delta\tau$-delayed version $\mathcal{T}_{\text{meas}} = \Delta\tau + \mathcal{T}_{\text{ref}}$.
- Calculate the Fourier transform of the reference and measurement impulse response traces, $r_{\text{ref}}(t)$ and $r_{\text{meas}}(t)$, time-windowed over $\mathcal{T}_{\text{ref}}$ and $\mathcal{T}_{\text{meas}}$, respectively, as $R_{\text{ref}}(f) = \mathcal{F}[r_{\text{ref}}(\mathcal{T}_{\text{ref}})]$ and $R_{\text{meas}}(f) = \mathcal{F}[r_{\text{meas}}(\mathcal{T}_{\text{meas}})]$.

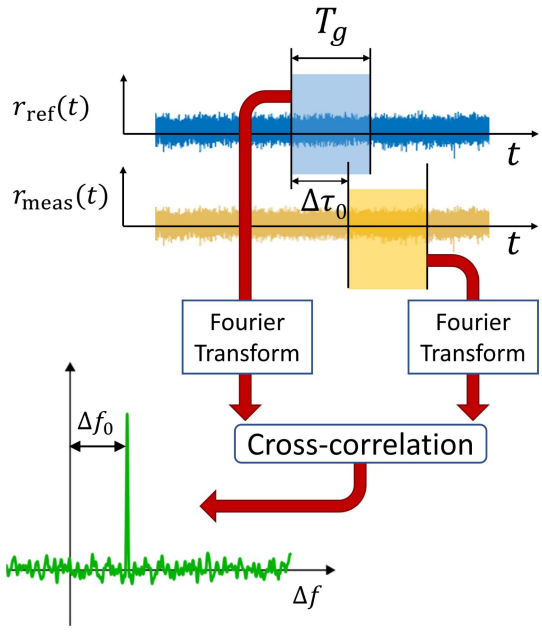

Fig. 1. Graphical representation of the SCA method. The method relies on the cross-correlation between the Fourier transform of the T_g-windowed trace $r_{\text{ref}}(t)$ and the trace $r_{\text{ref}}(t)$, opportunely delay by an interval $\Delta\tau_0$ which maximizes the correlation. The time windows, shown as shaded areas in the two traces, identify the same portion of the fiber. These two delayed time widows, upon cross-correlation, reveal a frequency shift Δf_0, which is related to the perturbation that section underwent between the two measurements.

- Calculate the cross-correlation between the spectra of the time-window impulse responses as $\mathcal{C}(\mathcal{T}_{\text{ref}}, \mathcal{T}_{\text{meas}}, \Delta f) = R_{\text{ref}} \star R_{\text{meas}}$. Note that, for a given T_g, $\mathcal{C}(\mathcal{T}_{\text{ref}}, \mathcal{T}_{\text{meas}}, \Delta f) \equiv \mathcal{C}(t, \Delta\tau, \Delta f)$ is indeed a three-dimensional dataset, which ultimately depends on the roundtrip time t (i.e., position $z = v_g t/2$ along the fiber on the reference trace), $\Delta\tau$ (i.e., temporal, and hence spatial, misalignment between the sections analyzed in the two traces), and the frequency shift Δf. For convenience, we will therefore refer to this dataset as $\mathcal{C}(z, \Delta\tau, \Delta f)$.
- Based on the uniqueness of the local Rayleigh signature, for each point $z = v_g t/2$ on the reference trace, there exists a delay, $\Delta\tau_0$, and a frequency shift, Δf_0, for which the cross-correlation dataset shows a marked peak (in absolute value). It also means that the measurements of the same physical section of sensing fiber are time-delayed by $\Delta\tau_0$ across the two sessions. Or equivalently, the two traces are spatially misaligned of $v_g\Delta\tau_0/2$. Moreover, owing to (2), this means that the fiber section, $v_g T_g/2$-long, beginning at the position z of the reference trace (i.e., $z' = z + v_g\Delta\tau_0/2$ in the measurement trace) underwent a change either in temperature or strain between the two sessions.

It is worthwhile noticing that the SCA method is highly versatile since it does not require the two measurements to share a common absolute time-spatial domain, unlike commercial and standard spectral analysis implementations [18]. Suppose the reference and measurement traces are collected using patchcords of different lengths between the interrogator and the sensing fiber. In that case, the method can identify the proper delay $\Delta\tau_0$, which aligns the two traces at the sensing fiber and allows for a consistent cross-correlation. Moreover, if the delay changes due to any other possible event, e.g., a resplicing of a damaged sensing fiber, the method will recover the alignment. Its versatility and robustness have also been demonstrated in other kinds of measurements [14], [19], [20], normally impossible with conventional spectral analysis. This versatility comes, however, at the cost of a high computational effort, which, in this case, is strongly impacted by the interval of possible delay values $\Delta\tau$ where the tridimensional correlation function $C(t, \Delta\tau, \Delta\omega)$ is calculated. Nonetheless, the interval of delays can be limited in most cases to a narrow range around an opportune educated guess, given by any distinguishable event in the portion of the trace corresponding to the sensing fiber and common to both traces. Some possible events that can be used to estimate the delay between the two traces include the front connector peak, splices, and Fresnel peak. By doing this, computational times can be limited from a few seconds at coarse spatial resolutions to several minutes per meter of fiber at a more detailed resolution.

As per standard OFDR data analysis, the impulse response is sampled with a raw time resolution δt, determined by the bandwidth $\Delta\lambda$ scanned by the tunable laser of the OFDR device. In particular, it reads $\delta t \approx \lambda_0^2/(c_0\Delta\lambda)$, where λ_0 is the central wavelength. Moreover, the maximum measurable frequency shift is given by $1/\delta t$. On the contrary, the spatial resolution of the spectral correlation, Δz, is determined by the time window length T_g used in the analysis as $\Delta z = T_g c_0/(2n)$. The time window length T_g also determines the resolution δf on the spectral shift measurement, which reads $\delta f = 1/T_g$. For example, the measurements presented in this work have been collected over a bandwidth of approximately 42 nm centered around 1550 nm. This corresponds to a raw sampling time δt of approximately 0.19 ps. With a time window of analysis consisting of 512 points (i.e., $T_g \approx 97.7ps$), which are also the number of points used for the correlation, the corresponding spatial resolution is $\Delta z \approx 1cm$ and the frequency resolution is $\delta f \approx 10$ GHz. This frequency resolution corresponds to an equivalent strain and temperature resolution of 67 $\mu\varepsilon$ and 8 °C, respectively. As one can note, this example shows that high-resolved spectral measurements come at the cost of a coarse spatial resolution. To address this limitation, it is possible to zero-pad the signal $r_{\text{ref}}(\mathcal{T}_{\text{ref}})$ and $r_{\text{meas}}(\mathcal{T}_{\text{meas}})$ before performing the Fourier transform [21]. Without zero-padding, the correlation peak may consist of only one sample. Upsampling makes the peaks smoother while keeping the same time window length T_g, and the detection of their position is more accurate. Consequently, the resolution for detecting the frequency of the correlation peak is enhanced while keeping the spatial resolution at reasonably low values. It is also worth noticing that this feature makes the analysis more robust against measurements with high spatial strain or temperature spatial gradient, which requires short spatial resolution to follow the spectral shift evolution consistently without impacting the quality of the analysis [22], [23].

The last point to address is the quality of the measurements obtained by applying SCA to the traces collected in challenging

conditions, such as those addressed. This quality is inherently related to the strength of the cross-correlation operation: the wider and the lower the cross-correlation peak, the worse the quality of the correlation analysis. This quality factor, Q, is therefore here defined as:

$$Q(z) = \left(1 - \frac{\text{mean}_{\Delta f \neq \Delta f_0} |\mathcal{C}(z, \Delta\tau_0, \Delta f)|}{|\mathcal{C}(z, \Delta\tau_0, \Delta f_0)|}\right) \times 100\%, \quad (6)$$

which is the percentage deviation from the unity of the mean cross-correlation floor at the optimal delay $\Delta\tau_0$, normalized to its maximum value. Note that this quality factor is affected by the spatial resolution. Indeed, by decreasing the window length T_g, the main peak of the spectral correlation becomes broader and lower, and additional side lobes may appear and become larger [24]. At the same time, shorter windows should be capable of following high spatial strain/temperature gradients.

III. Experimental Results

The results presented in this section are obtained from raw measurements taken with commercial OFDR interrogators (Luna OBR4600©, Luna Inc., Roanoke, VA, USA), taken from two different sites. This device measures the backscattered signal on two orthogonal polarization axes; therefore, it is possible to perform SCA between each signal polarization, leading to four possible tri-dimensional datasets. In particular, for each of the measurements presented here, we have selected the combination of polarizations at each point that resulted in the largest cross-correlation. Moreover, all the measurements shown here have been collected over a wavelength bandwidth of approx. 42 nm, corresponding to a raw-sampling time of ≈ 0.19 ps.

The first site is a steel-tied-arch bridge located in Treviso, Italy. During the construction in 2016, fibers were embedded in a foundation pile at this location [25]. The second site is a landslide in Tuscany, Italy, which was instrumented with fiber-equipped soil anchors with external concrete slabs in 2018 [26].

We conducted measurement campaigns on these sites to gather geotechnical and civil engineering data for the monitored structures. However, these campaigns have been interrupted over the years due to the changes of both the interrogator and the connecting patchcords. These changes have impeded the analysis of current traces while keeping the original reference using the standard approach and commercial software, as the associated misalignment completely inhibits the analysis. However, as will be seen in the following, the SCA analysis confirmed the persistence of the Rayleigh signature, overcoming this issue.

In the following subsection, we present data collected from commercial strain- and temperature-sensing cables for each site. Fig. 2 shows the cross-section of these cables: they are widely used in different sensing applications [27], [28], and they both integrate a steel tube hosting single-mode fibers and an engineered outer sheath. The fiber coupling within the tube and the sheath differ depending on the sensing parameter of interest.

A single fiber is rigidly encapsulated within the tube of the strain-sensing cable to ensure an effective strain transfer from the outer sheath. In turn, the plastic outer sheath is corrugated for better adhesion with the surrounding material, which is concrete

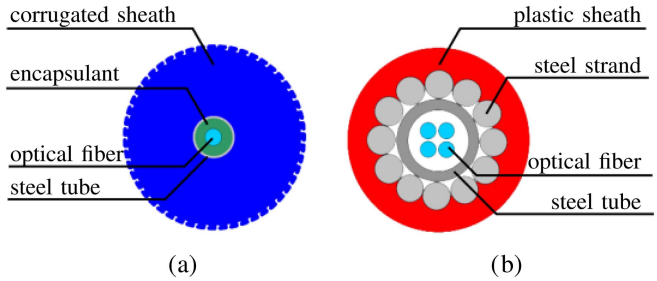

Fig. 2. Cross-section sketches of cables of this work: (a) strain (Solifos BRUsens v9 DSS) and (b) temperature sensing (Solifos BRUsens DTS).

in both sites (Fig. 2(a)). Instead, the temperature-sensing cable may embed more than one fiber, hosted in a loose configuration within the tube, filled with a thixotropic gel compound. The outer sheath is made of steel strands surrounded by a plastic smooth layer (Fig. 2(b)). This different structure is intended to insulate the inner fiber and prevent the strain cross-sensitivity mechanically.

At the same time, fibers embedded in strain-sensing cables are intrinsically exposed to significant stress during manufacturing, resulting in a faint residual stress. For this reason, the frequency shift measured by these cables is usually not as smooth as that of a temperature cable.

Please note that, for better comprehension, the following results are presented in terms of strain and temperature variation with respect to the reference measurement unless otherwise stated. In doing so, we have applied the gage factors of (4), which have been shown to provide consistent data for large strain applied to the cables, even beyond the elastic limit of the silica [29]. In this sense, the presence of a highly correlated signature guarantees that the measurement can be done and that the values of strain and temperature are consistent and valid. However, interpreting the strain and temperature variation for geotechnical purposes is beyond the scope of this work.

A. Measurements on Fibers in a Foundation Pile

In this site, three cables for strain sensing and one for the temperature, each 20 m long, are embedded in a single foundation concrete pile, part of a bridge abutment raft foundation [25], [26].

The following traces have been considered for this site:

- The reference traces were collected in October 2016 after the completion of the concrete abutment structure.
- An additional set of traces was collected in May 2017 after the full construction of the bridge. These traces, presented here as a control set, have been taken with the same device and setup as the reference traces.
- A final set of traces was measured in June 2023, almost seven years after the corresponding reference traces. A different device was used in this session, and the sensing cables were connected to the interrogator with a different patchcord. Moreover, the central wavelength varied by almost 2 nm between the two sessions. Therefore, the traces

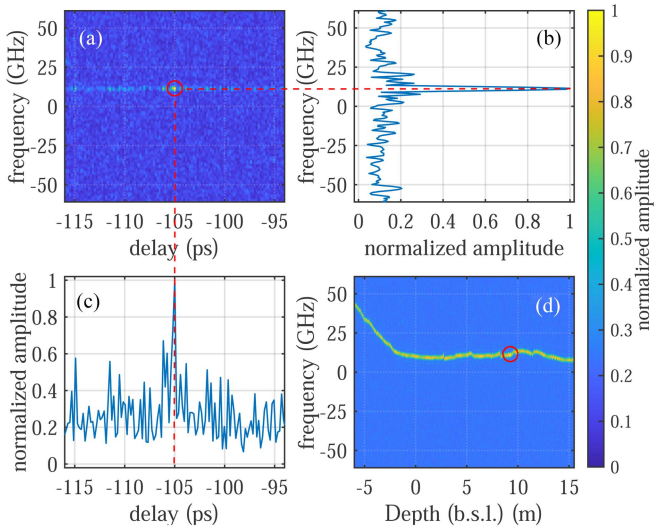

Fig. 3. Data from one of the strain cables integrated within a bridge foundation pile (measurement taken on June 2023, reference taken on Oct. 2016): (a) Contour map of the normalized amplitude of $\mathcal{C}(z_0, \Delta\tau, \Delta f)$ at an arbitrary point z_0. The maximum peak is located at $(\Delta\tau_0, \Delta f_0)$ (red circle). (b) Normalized cross-correlation amplitude $|\mathcal{C}(t_0, \Delta\tau_0, \Delta f)|$ at optimal delay. (c) Normalized cross-correlation amplitude $|\mathcal{C}(t_0, \Delta\tau, \Delta f_0)|$ at optimal frequency shift. (d) Contour map of the normalized amplitude versus position along the fiber (i.e., depth below sea level) for the optimal delays calculated at each position. The red circle in the plot represents the point z_0.

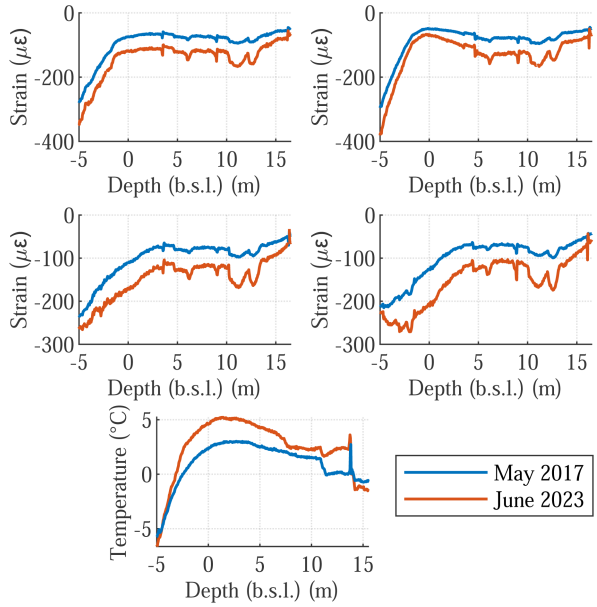

Fig. 4. Strain measured at the first site with four strain cables and one temperature cable as a function of the depth below sea level (b.s.l.). The blue and red curves refer to measurements collected in May 2017 and June 2023, respectively. The reference measurements for these curves were taken in Oct. 2016.

were collected over a slightly different wavelength range and did not share the same spatial axis as the references.

Fig. 3 shows an example of SCA analysis applied to one of the traces of the final set of measures. Fig. 3(a) displays the contour map of the normalized amplitude $|\mathcal{C}(z_0, \Delta\tau, \Delta f)|$ corresponding to an arbitrary point z_0 along the sensing fiber. The peak of this map (red circle of Fig. 3(a)) identifies the unique delay and the frequency shift, which best correlates the Rayleigh signature among the reference trace and the properly time-delayed measurement trace around this point (dashed lines from subplot a) to subplots b) and c)). The normalized amplitude curves at optimal delay and frequency shift, as a function of the frequency and delay, are represented in Fig. 3(b) and (c), respectively. Finally, Fig. 3(d) displays the contour map of the amplitude dataset versus the position along the fiber obtained by selecting the optimal delay for each point. The red circle in the plot identifies the point z_0 analyzed in subplots a)-c). The locus of the cross-correlation maximum represented by the contour map of subplot d) identifies the strain along the cable.

The data collected in this first site are represented in Fig. 4. As stated above, the spectral shifts are represented in terms of strain and temperature variation, using the gage factor of (4). The blue curves were collected one year after the reference in a favorable condition, i.e., using the same interrogator and optical setup. The red curves collected more than six years later were measured with a different interrogator and patch cord from the interrogator to the sensing cables: the capability of doing these measurements solely relies on the actual persistence of the Rayleigh fingerprint of the sensing fibers.

The spatial resolution for these measurements has been chosen so that the quality factor (6) is not less than 50% all along the sensing cable. In this case, all traces have been obtained with a spatial resolution of approx. 8 cm, and a distance among sampling points of ≈4 cm. The corresponding raw spectral resolution is approx. 1.28 GHz; yet, an upsampling has been applied, leading to sub-$\mu\varepsilon$ and less than one tenth of °C resolution. As one can see, each strain profile shows a slightly increasing cable contraction over time with respect to the reference trace, with common well-localized features among the two measurements. The curves collected with the temperature cable are smoother due to the loose configuration of the fiber in the cable; still, common events are clearly identified along the cable.

The effect of the spatial resolution on the analysis is investigated in Fig. 5 for the measurement of June 2023 collected from one of the strain cables. Fig. 5 shows, on the left, the strain profile collected from the cable for two different spatial resolutions, i.e., 4 cm (upper plot) and 8 cm (lower plot). On the right, Fig. 5 shows the corresponding quality factor $Q(z)$. The outlier peaks in the uppermost strain profile ("strain reading anomalies" [30]) have been clipped to make the plot readable. These anomalies correspond to points along the fiber for which the correlation analysis has failed to determine the spectral shift of the peak and for which the quality factor is locally less than 40%. Relaxing the spatial resolution to a larger value makes the correlation more robust, and the outliers disappear. Therefore, the best-averaged quality (around 70%) is obtained, in this example, at a coarser spatial resolution (lower plots of Fig. 5). For small strain and strain gradient values, like those measured here, the correlation analysis benefits from a longer time window [24]. Please also note that despite the quality factor obtained for the smaller spatial

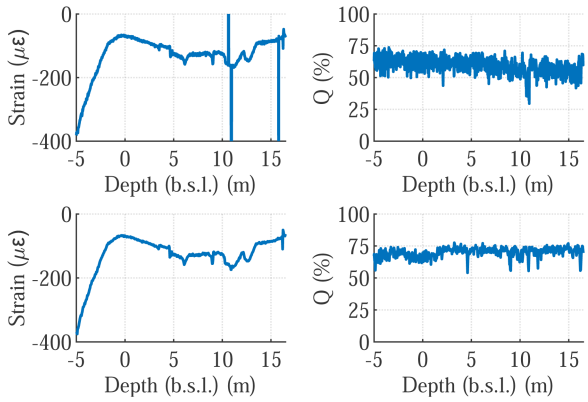

Fig. 5. Strain (on the left) and corresponding quality factor (on the right) measured on June 2023 at the first site with one of the strain cables for a spatial resolution of 4 cm (upper plots) and 8 cm (lower plots).

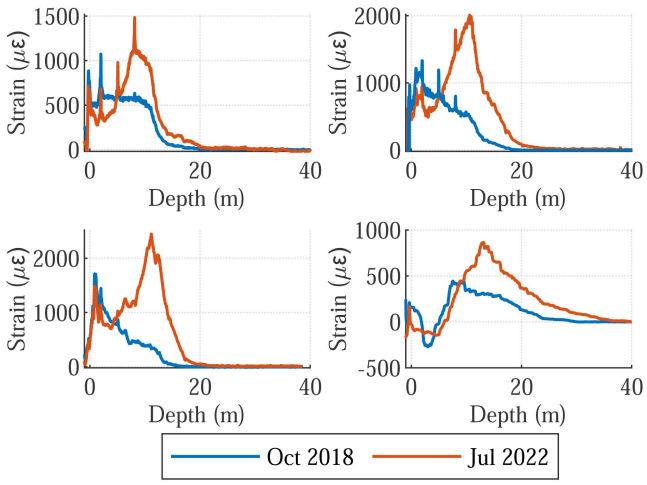

Fig. 6. Strain measured at the second site with four cables. The blue and red curves refer to measurements collected in Oct. 2018 and Jul. 2022, respectively. The reference measurements for these curves were taken in June 2018.

resolution being degraded, it is still possible to retrieve the strain with sufficient accuracy if one tolerates sparse strain reading anomalies.

Despite the many years of challenging conditions and the change in the measurement setup (interrogator and patch cord), the correlation's high quality confirms the Rayleigh signature's persistence.

B. Measurements on Fibers in Soil Anchors

At the second site, three soil anchors equipped with fiber-optic cables are installed to stabilize a landslide-prone area. Each anchor is approximately 40 meters long, with an optical cable embedded for strain sensing.

These anchors are threaded hollow bars that embed the fibers within the concrete. The installation involves forcefully pushing the bar into the ground in sections, lowering one or more fibers into the inner hole using a steel tendon for support, and pouring concrete to couple the fiber and the tendon to the bar [29]. One of the anchors of this site has also been equipped with an additional cable for temperature measurement, with the fiber in a loose configuration within the metal tube. Unfortunately, this cable was squeezed during the installation, resulting in a partial yet dominant mechanical coupling. For this reason, the data from this cable has been represented in terms of strain, using the k_ε coefficient of (4). Although the actual data provided by this cable is not relevant for monitoring, they still allow us to verify the persistence of the Rayleigh backscattering.

In this site, the following traces have been considered:

- The reference traces were collected in June 2018 after the complete cure of the concrete.
- A set of traces (taken on Oct. 2018) some months after the anchors were tensioned through a hydraulic piston, which applied a certain pulling force against the ground. This operation is intended to "activate" the frictional forces at the soil-anchor interface. These traces share the same device and setup as the reference traces, except for the fiber in the strain cable of one of the anchors, which was respliced because it was damaged at the end of the tensioning mentioned above. On that occasion, a new reference was taken right after the resplice to guarantee the continuity of the subsequent measurements with the proprietary software. The strain of that cable, with respect to the reference of June 2018, was then iteratively calculated as the sum of the strain variation with respect to the measurement taken after the resplice with the strain variation measured just before the resplice, with respect to June 2018.
- The most recent set of traces was collected in July 2022, four years after the corresponding reference traces, with a different interrogator with a slightly different wavelength range and a different patchcord.

As per the previous site, blue curves were collected soon after the reference, while red ones were collected after more than four years. The right upper plot refers to the cable respliced after the tensioning, and both curves have different spatial alignments with respect to the reference traces. Instead, the lowermost right graph refers to the strain collected on the loose-type cable, initially intended for temperature sensing. The spatial resolution was chosen for each cable so that the quality factor was larger than 50% across measurement sessions and without spectral reading anomalies. Following this approach, the spatial resolutions at which the strain was calculated for each cable were 2, 8, 4, and 8 cm, respectively. Differently from the previous site, the analysis here is performed at different spatial resolutions for the different cables. This is understandable in light of the conditions in which these fibers are exposed. Indeed, the strain exerted on the cable is here determined by the action of the landslide transferred to the anchor and, in turn, to the cable via the shear friction, and, therefore, depends also on the surrounding soil. Despite the anchors being deployed in the same site, the condition is unlikely to be the same, as the way in which the landslide is evolving may differ from point to point and soil layer to soil layer. This leads to more variable effects on Rayleigh's persistence. As with the previous site measurements, oversampling was applied, and the resolution in strain was no larger than 2 $\mu\varepsilon$ for each of the measurements.

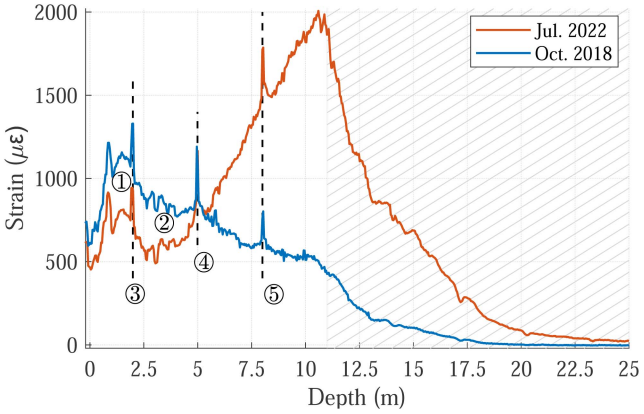

Fig. 7. Strain curve measured at the second anchor of the second site (magnification of right uppermost graph of Fig. 6): Circled numbers refer to the most visible common features in strain pattern. The hatched region corresponds to the bedrock.

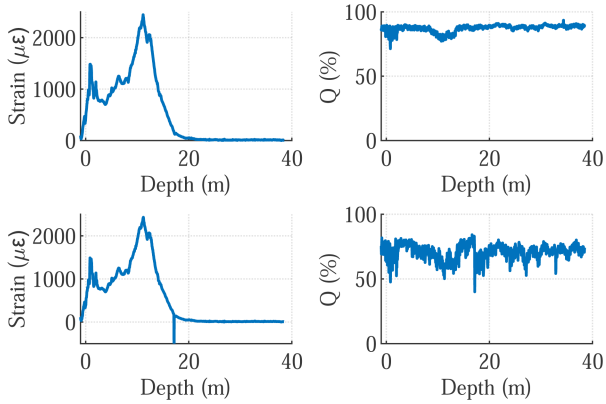

Fig. 8. Strain (on the left) and corresponding quality factor (on the right) measured on July 2022 at the second site with one of the strain cables for a spatial resolution of 4 cm (upper plots) and 8 cm (lower plots).

One can observe a marked additional strain in all the cables, including the loose-type one. This is caused by the active landslide, whose sliding surface crosses the bar at a depth around 10–12 m. Below that depth, the anchors penetrate the bedrock. As a matter of fact, the operative conditions to which these fibers are exposed at this site are incredibly harsh. These operative conditions, especially at the sliding surface, are so extreme that one may wonder if the anchor is still properly coupled to the surrounding soil or if the embedded cable is still working properly (e.g., no slippage between the cable's inner layers occurs), resulting in altered strain transfer. However, this may also happen in the case of a faulty cable, a wrong installation of the cable within the anchor, or of the anchor within the ground. Although relevant for the final users, this paper does not investigate these aspects.

Again, the persistence of the Rayleigh fingerprint testified by the marked cross-correlation allows us to perform the measurements. In addition, the strain curves collected at the two sessions show marked similarities, in particular for the two uppermost plots. For example, Fig. 7 shows a magnification view of the right-uppermost plot, where the most evident common patterns in the strain profile, among the many, are identified by circled numbers. These curves contain a richness of details: in particular, one can note the strain patterns around 1.5 m (①) and 3.5 m (②).

The common well-localized peaks, identified by ③, ④, and ⑤, are instead referable to the interplay at the couplings nuts of the bars [29]. Additional, less evident similarities can be identified within the bedrock substrate (hatched region of the plot). Even well-localized events can be accurately detected and traced, further confirming the persistent Rayleigh signature of the fibers.

Similarly, Fig. 8 shows an example of the effect of different spatial resolutions on the quality factor and the collected traces. The curves refer to the more recent measurement session on anchor 3. The uppermost plots are calculated at a spatial resolution of 4 cm, while the lowermost at 8 cm. Differently from the previous site, the average quality diminishes at the coarser spatial resolution, and a strain reading anomaly appears. Indeed, the high spatial strain gradient to which this fiber is exposed is better measured with a short spectral correlation window. In fact, analyses carried out at small spatial resolution are generally better able to follow the strain's fast spatial gradient.

Please note that although the quality of the measurements has degraded over the years, we have not observed any evident degradation in the propagation properties, such as increased attenuation. Of course, we expect both the rate at which this degradation occurs and the attenuation to be affected by the conditions at which the fibers are exposed. Nonetheless, how these two aging phenomena are related is not, at the moment, clear.

IV. Conclusion

This work investigates the persistence of Rayleigh signature in fibers employed in harsh conditions by analyzing measurements collected with fibers embedded in a foundation pile and soil anchors exposed to an active landslide.

It is shown that a proper spectral correlation analysis can still reveal and consistently correlate the Rayleigh fingerprint between measurements over more than six years, even if different interrogators and setups are employed to collect the raw measurements.

In conclusion, our analysis definitely confirms the persistence of Rayleigh's signature of the fibers over many years, even in the harshest conditions. We believe that this represents a crucial step toward using Rayleigh-based monitoring for long-term campaigns, for which the interrogator or the connecting patchcords may change over the years. In this sense, it could enable precise and robust long-term referencing of Rayleigh measurements. Furthermore, this work paves the way for further promoting the Rayleigh signature as an inherent characteristic associated with each unique fiber, regardless of the device or setup used for measurements.

Acknowledgment

The authors acknowledge Eng. Bergamo Otello and Veneto Strade SpA for the logistic support on the measurements campaign on the first site.

REFERENCES

[1] L. Palmieri and L. Schenato, "Distributed optical fiber sensing based on rayleigh scattering," *Open Opt. J.*, vol. 7, pp. 104–127, 2013.

[2] L. Palmieri, L. Schenato, M. Santagiustina, and A. Galtarossa, "Rayleigh-based distributed optical fiber sensing," *Sensors*, vol. 22, no. 18, 2022, Art. no. 6811.

[3] B. J. Soller, M. E. Froggatt, D. K. Gifford, and M. S. Wolfe, "Fiber keying for optical network intrusion monitoring," in *Proc. Opt. Solutions Homeland Nat. Secur.*, 2005, Paper P2.

[4] D. K. Gifford and M. E. Froggatt, "Rayleigh scatter based high resolution distributed fiber sensing for safety and security applications," in *Proc. Front. in Opt.*, 2013, Paper FW4I.2.

[5] Y. Du, S. Jothibasu, Y. Zhuang, C. Zhu, and J. Huang, "Unclonable optical fiber identification based on rayleigh backscattering signatures," *J. Lightw. Technol.*, vol. 35, no. 21, pp. 4634–4640, Nov. 2017.

[6] M. Froggatt and J. Moore, "High-spatial-resolution distributed strain measurement in optical fiber with rayleigh scatter," *Appl. Opt.*, vol. 37, no. 10, pp. 1735–1740, Apr. 1998.

[7] B. J. Soller, D. K. Gifford, M. S. Wolfe, and M. E. Froggatt, "High resolution optical frequency domain reflectometry for characterization of components and assemblies," *Opt. Exp.*, vol. 13, no. 2, pp. 666–674, Jan. 2005.

[8] R. G. Duncan et al., "OFDR-based distributed sensing and fault detection for single-and multi-mode avionics fiber-optics," in *Proc. 10th Joint Conf. Aging Aircr.*, 2007.

[9] M. F. Bado, J. R. Casas, and J. Gómez, "Post-processing algorithms for distributed optical fiber sensing in structural health monitoring applications," *Struct. Health Monit.*, vol. 20, no. 2, pp. 661–680, Jun. 2020.

[10] D. C. Sweeney, A. M. Schrell, and C. M. Petrie, "An adaptive reference scheme to extend the functional range of optical backscatter reflectometry in extreme environments," *IEEE Sensors J.*, vol. 21, no. 1, pp. 498–509, Jan. 2021.

[11] U. M. N. Jayawickrema, H. M. C. M. Herath, N. K. Hettarachchi, H. P. Sooryaarachchi, S. Baneryee, and J. A. Epaarachchi, "Impact of spectral shift quality (SSQ) on fiber optic sensor readings in reinforced concrete beams," in *Proc. 14th Int. Workshop Struct. Health Monit.*,, 2023.

[12] M. E. Froggatt and D. K. Gifford, "Rayleigh backscattering signatures of optical fibers—Their properties and applications," in *Proc. Opt. Fiber Commun. Conf. Expo. Nat. Fiber Optic Engineers Conf.*, 2013, pp. 1–3.

[13] L. Schenato, et al., "On the long-term persistence of rayleigh signature of optical fibres in harsh conditions," in *Proc. 28th Int. Conf. Opt. Fiber Sensors*, 2024, Paper Tu5.3.

[14] R. Veronese, A. Galtarossa, and L. Palmieri, "Distributed characterization of few-mode fibers based on optical frequency domain reflectometry," *J. Lightw. Technol.*, vol. 38, no. 17, pp. 4843–4849, Sep. 2020.

[15] J. P. von der Weid, R. Passy, G. Mussi, and N. Gisin, "On the characterization of optical fiber network components with optical frequency domain reflectometry," *J. Lightw. Technol.*, vol. 15, pp. 1131–1141, Jul. 1997.

[16] X. Wang, W. Li, L. Chen, and X. Bao, "Thermal and mechanical properties of tapered single mode fiber measured by OFDR and its application for high-sensitivity force measurement," *Opt. Exp.*, vol. 20, no. 14, pp. 14779–14788, Jul. 2012.

[17] H. Boiron et al., "Optical fiber strain and temperature coefficients determination based on Rayleigh-OFDR," in *Opt. Fiber Sensors Conf. Special Ed.*, 2020, p. T3.42.

[18] C. Liang, Q. Bai, M. Yan, Y. Wang, H. Zhang, and B. Jin, "A comprehensive study of optical frequency domain reflectometry," *IEEE Access*, vol. 9, pp. 41647–41668, 2021.

[19] R. Veronese et al., "Experimental characterization of group and phase delays induced by bending and twisting in multi-core fibers," *Opt. Lett.*, vol. 46, no. 11, May 2021, Art. no. 2674.

[20] M. Cappelletti et al., "Distributed fiber optic shape sensing with simultaneous interrogation of multiple fibers based on rayleigh-signature domain multiplexing," *Opt. Lett.*, vol. 48, no. 22, Nov. 2023, Art. no. 5907.

[21] J. Cui, S. Zhao, D. Yang, and Z. Ding, "Investigation of the interpolation method to improve the distributed strain measurement accuracy in optical frequency domain reflectometry systems," *Appl. Opt.*, vol. 57, no. 6, pp. 1424–1431, Feb. 2018.

[22] A. Barrias, J. R. Casas, and S. Villalba, "Embedded distributed optical fiber sensors in reinforced concrete structures-a case study," *Sensors*, vol. 18, no. 4, 2018, Art. no. 980.

[23] L. Suo, Z. Lei, S. Zhao, Z. Wu, and A. Takezawa, "Study on sliding-window length based on rayleigh backscattering spectrum correlation in distributed optical-fiber strain measurement," *Opt. Fiber Technol.*, vol. 47, pp. 126–132, Jan. 2019.

[24] S. Zhao, J. Cui, Z. Wu, and J. Tan, "Accuracy improvement in OFDR-based distributed sensing system by image processing," *Opt. Lasers Eng.*, vol. 124, Jan. 2020, Art. no. 105824.

[25] S. Bersan, O. Bergamo, L. Palmieri, L. Schenato, and P. Simonini, "Distributed strain measurements in a CFA pile using high spatial resolution fibre optic sensors," *Eng. Structures*, vol. 160, pp. 554–565, 2018.

[26] S. Cola et al., "On distributed strains in a CFA pile via DFOSs measurements and numerical analysis," in *Proc. XVII Eur. Conf. Soil Mechanics Geotechnical Eng.*, 2019, pp. 3508–3515.

[27] L. Schenato et al., "Distributed optical fibre sensing for early detection of shallow landslides triggering," *Sci. Rep.*, vol. 7, no. 1, 2017, Art. no. 14686.

[28] C. M. Monsberger, W. Lienhart, and M. Hayden, "Distributed fiber optic sensing along driven ductile piles: Design, sensor installation and monitoring benefits," *J. Civil Struct. Health Monit.*, vol. 10, no. 4, pp. 627–637, Jun. 2020.

[29] S. Cola et al., "Composite anchors for slope stabilisation: Monitoring of their in-situ behaviour with optical fibre," *Geosciences*, vol. 9, no. 5, 2019, Art. no. 240.

[30] M. F. Bado, J. R. Casas, and A. Barrias, "Performance of rayleigh-based distributed optical fiber sensors bonded to reinforcing bars in bending," *Sensors*, vol. 18, no. 9, 2018, Art. no. 3125.

Open Access provided by 'Università degli Studi di Padova' di Studi Universitari e di Perfezionamento' within the CRUI CARE Agreement